NJC

Accepted Manuscript

This is an *Accepted Manuscript*, which has been through the Royal Society of Chemistry peer review process and has been accepted for publication.

Accepted Manuscripts are published online shortly after acceptance, before technical editing, formatting and proof reading. Using this free service, authors can make their results available to the community, in citable form, before we publish the edited article. We will replace this *Accepted Manuscript* with the edited and formatted *Advance Article* as soon as it is available.

You can find more information about *Accepted Manuscripts* in the Information for Authors.

Please note that technical editing may introduce minor changes to the text and/or graphics, which may alter content. The journal's standard Terms & Conditions and the Ethical guidelines still apply. In no event shall the Royal Society of Chemistry be held responsible for any errors or omissions in this *Accepted Manuscript* or any consequences arising from the use of any information it contains.

ROYAL SOCIETY OF CHEMISTRY

www.rsc.org/njc

NJC

RSCPublishing

ARTICLE

Highly ordered mesoporous $Cd_xZn_{1-x}Se$ ternary compound semiconductors with controlled band gap energies†

Cite this: DOI: 10.1039/x0xx00000x

Received 00th April 2014,
Accepted 00th April 2014

DOI: 10.1039/x0xx00000x

www.rsc.org/

Yoon Yun Lee,[a] Jeong Kuk Shon,[b,‡,*] Suyeon Bae,[c] Xing Jin,[b] Yeong Jin Choi,[b,d] Sun Sang Kwon,[b] Tae Hee Han,[e] and Ji Man Kim[a,b,c,*]

Highly ordered mesoporous compound semiconductors ($Cd_xZn_{1-x}Se$) with crystalline frameworks were successfully synthesized *via* a nano-replication method from a mesoporous silica template (bicontinuous 3-D cubic *Ia3d* mesostructure, KIT-6). Simple impregnation with various molar compositions of the precursors within mesopores of the silica template, reduction at 500 °C under hydrogen atmospheres and subsequent removal of silica template using NaOH solution resulted in the mesoporous $Cd_xZn_{1-x}Se$ ternary compound semiconductor. The mesoporous $Cd_xZn_{1-x}Se$ materials exhibiting high surface areas (90 – 120 m^2g^{-1}) were investigated by X-ray diffraction, N_2 adsorption-desorption, electron microscopy, and UV-visible spectroscopy. The unique optical properties and band gap profiles of the template-free $Cd_xZn_{1-x}Se$ materials were controlled chemically by different Cd/Zn molar composition, and also physically by framework thickness. Diffuse reflectance UV-visible studies indicate that the band gap energies (E_g) of the mesoporous $Cd_xZn_{1-x}Se$ materials widened as the amount of Cd decreased. Decreasing the framework thickness also results in the band gap widening of the mesoporous $Cd_{0.5}Zn_{0.5}Se$ materials due to nano-size effect.

1. Introduction

Recently, many researchers have been focused on the synthesis and application of nanostructured materials such as nanoparticles, nanotubes, nanowires, nanorods and nanosheets.[1-4] Mesoporous materials, exhibiting uniform pore size, ordered porous structures and high surface areas, have also widely investigated due to their unique properties that are applicable in the fields of adsorbent, catalysis, catalyst supports, energy materials and so on.[5-9] From the early to the late 1990s, the mesoporous silica materials with various ordered pore structures, morphologies and particle sizes have been mainly studied.[10-16] However, due to the limitation of silica-based materials, non-silicious mesoporous materials such as carbons, metals or metal oxides have attracted much attention. Since the late 1990s, a nano-replication (hard-templating) approach has been adapted to produce ordered mesoporous materials with non-siliceous frameworks using ordered mesoporous silica materials as hard-templates.[17-28]

There have been great interest in the synthesis and application of nanostructured metal chalcogenide compounds such as ZnE, CdE, PbE and CuE (E = S, Se, and Te), because of their unique optical and physicochemical properties. Especially, the II-group metal, based chalcogenide compounds, have been widely investigated for the applications in electronic and optoelectronic devices such as photovoltaics, light-emitting diodes and laser diodes [29]. Due to these properties, plenty of studies were reported in the fields of metal chalcogenide compound semiconductor materials which have spherical shape, tetrapod nanostructure, nanorods, nanowires and/or other nanomaterials.[30-36] The ordered mesoporous semiconductor materials with crystalline framework are also expected to provide new possibilities for some applications in the fields of energy, catalysis and other optoelectronic devices. However, there have been only a few examples of the ordered mesoporous compound semiconductors that consist of II, III, V and VI group elements were reported.[37, 38] The II-group metal based chalcogenide compounds with ordered mesoporous structure were seldom reported until now.[38, 39]

II-VI compound semiconductors with wide band gaps, such as CdSe and ZnSe, are well-known as most important compound semiconductor materials due to their unique semiconducting properties.[40-43] These are considered as suitable materials for organic-inorganic hybrid solar cells and/or photocatalysis due to their band gap energy and band structure.[44, 45] However, typically, nano-sized CdSe or ZnSe materials prepared by using toxic organo-metallic precursors such as dimethylcadmium ($Cd(CH_3)_2$) and/or diethylzinc

($Zn(C_2H_5)_2$) which is very harmful for the environment.[46, 47] Furthermore, due to physicochemical and optical property of semiconductors are mostly influenced by band gap energy, the band gap tuning of semiconductors would be very important for their practical applications. However, due to the scarcity of suitable precursors, ordered mesoporous metal selenide has not been reported up to now.[39]

In the present work, we report on a facile synthesis route to highly ordered mesoporous $Cd_xZn_{1-x}Se$ ternary compound semiconductors with different Cd/Zn molar ratios and controlled framework thicknesses by using cheap, readily available, and less harmful for the environment precursors of cadmium nitrate ($Cd(NO_3)_2{\cdot}4H_2O$), zinc nitrate ($Zn(NO_3)_2{\cdot}6H_2O$), and selenium oxide (SeO_2) *via* nano-replication using pore size controlled mesoporous silica KIT-6s (bicontinuous cubic *Ia*3*d* mesostructure) as hard-templates. The band gap energies of the mesoporous $Cd_xZn_{1-x}Se$ materials were finely tuned both chemically and physically by the framework composition and thickness variation.

2. Experimental

2.1 Preparation of KIT-6 template

Ordered mesoporous silica KIT-6, exhibiting 3-D cubic *Ia*3*d* mesostructures, were synthesized following the procedure described elsewhere.[48, 49] Pluronic triblock copolymer P123 ($EO_{20}PO_{70}EO_{20}$, Aldrich, MW = 5800) and tetraethyl orthosilicate (TEOS, Samchun Chemical, 98%) were utilized as the structure-directing agent and silica framework source, respectively. In a typical synthesis, 30 g of P123 polymer was dissolved in a mixture of 30 g of *n*-butanol (anhydrous, Aldrich, 99%), 59 g hydrochloric acid (HCl, Samchun Chemical, 35 – 37%) and 1085 g of doubly distilled water at the room temperature. The clear polymer solution was put in water bath at 35 °C and kept in the bath under vigorous stirring for more than 3 h in order to reach thermal equilibrium. Then, 64.5 g of TEOS was added in this polymer solution. The reaction mixture was vigorously stirred for 24 h at 35 °C, and subsequently kept for another 24 h in an oven at 100 °C under static conditions. The precipitate were filtered, dried and washed with distilled water. To remove the P123 polymer, the product was calcined in air at 550 °C for 3 h. In order to control the mesopore sizes of KIT-6 materials, the hydrothermal treatment after stirring at 35 °C for 24 h were carried out at the temperatures between 40 and 140 °C [48]. The silica templates, thus obtained, denoted as KIT-6-*t* where *t* is the hydrothermal treatment temperatures in Celsius degree (°C).

2.2 Synthesis of mesoporous $Cd_xZn_{1-x}Se$

Mesoporous $Cd_xZn_{1-x}Se$ ($x = 0 – 1$) materials were obtained *via* nano-replication method using the KIT-6 templates. Zinc nitrate hexahydrate ($Zn(NO_3)_2{\cdot}6H_2O$, Samchun Chemical, 98%), cadmium nitrate tetrahydrate ($Cd(NO_3)_2{\cdot}4H_2O$, Samchun Chemical, 98%) and selenium dioxide (SeO_2, Samchun Chemical, 99.8%) was used as received. In order to synthesize the mesoporous CdSe ($x = 1$), a solution containing 2.12 g of $Cd(NO_3)_2{\cdot}4H_2O$, 0.76 g of SeO_2 and 3.0 g of distilled water was infiltrated into mesopore of the KIT-6 template (3.0 g) *via* incipient wetness method. After drying at 80 °C oven for 12 h, the composite was heated to 500 °C for 3 h under hydrogen atmosphere. Subsequently, the hydrogen flow was changed with nitrogen flow, and the furnace was cooled down to 80 °C. The silica template was removed using 1 M NaOH aqueous solution three times. In case of synthesis of the mesoporous ZnSe, 2.05 g of $Zn(NO_3)_2{\cdot}6H_2O$ was used instead of $Cd(NO_3)_2{\cdot}4H_2O$. The mesoporous $Cd_xZn_{1-x}Se$ materials were prepared by same synthesis procedures described above with controlled molar composition between the metal precursors.

The $Cd_xZn_{1-x}Se$ materials, thus obtained, are denoted as CZS-*t*-*x* where the CZS means the $Cd_xZn_{1-x}Se$, *t* is the hydrothermal temperature of the KIT-6 templates in Celsius degree (°C), and *x* is the molar composition of cadmium in $Cd_xZn_{1-x}Se$ material.

2.3 Characterization

Powder X-ray diffraction (XRD) patterns were obtained in reflection mode using a Rikagu D/MAX-2200 Ultima equipped with Cu K_α radiation at 30 kV and 40 mA, and in transmittance mode using a Rigaku D/MAX-2500 equipped with Cu K_α radiation at 40 kV and 300 mA. Scanning electron microscope (SEM) images were taken using a LEO Supra 55 field emission scanning electron microscope (FE-SEM) operating at an accelerating voltage of 15 kV. High resolution SEM images were obtained using a Hitachi UHR S 5500 FE-SEM operating at 30 kV. Transmission electron microscope (TEM) images were obtained using a JEOL JEM 3010 at an accelerating voltage of 300 kV. N_2 adsorption-desorption isotherms were collected on a Micromeritics Tristar system at liquid N_2 temperature. All of the samples were completely dried under vacuum at 100 ^oC for 24 h before the measurement. The specific BET (Brunauer-Emmett-Teller) surface areas were calculated from the adsorption branches in the range of relative pressure (p/p_0) = 0.05 – 0.20. The pore size distribution curves were obtained by the BJH (Barrett-Joyner-Halenda) method on the basis of the adsorption branches. UV/visible absorption spectra were obtained from a Scinco S3100 UV-visible spectrometer.

3. Results and Discussion

3.1 Characterization of KIT-6 silica templates

The KIT-6-*t* silica materials, with 3-D cubic *Ia*3*d* mesostructures and different pore sizes, were used as the templates for the synthesis of CZS-*t*-*x* materials. Fig. 1 shows the XRD patterns and N_2 adsorption-desorption isotherms for the KIT-6-*t* silica templates. As shown in Fig. 1A, the first diffraction peak, which corresponds to (211) plane of cubic *Ia*3*d* mesostructure, are gradually shifted to lower angle region as the hydrothermal synthesis temperature increase from 40 to 140 °C. This peak shifting phenomenon is related to the increases of the *d*-spacing and lattice parameters of the KIT-6

silica templates. The N_2 sorption isotherms of the KIT-6 materials in Fig. 1B, synthesized at different hydrothermal temperature with type-IV hysteresis loop in the range of p/p_0 = 0.5 – 0.7 that are characteristics of the mesoporous material. The corresponding BJH pore size distributions are shown Fig. S1 (see supplementary information). As the hydrothermal temperature increases from 40 to 140 °C, the mesopore sizes periodically increased from 4.5 to 8.2 nm with linear relationship (inset of Fig. 1B, and table 1), but silica wall thicknesses were decreased from 5.2 to 3.3 nm. Total pore volumes of KIT-6 materials were also gradually increased from 0.43 to 0.92 cm^3g^{-1} with increases of the synthesis temperatures (Table 1). The representative morphologies of several micrometer sized particle and developed ordered mesostructures with uniform pore size of about 7 nm of the KIT-6-100 sample are presented in Fig. S2.

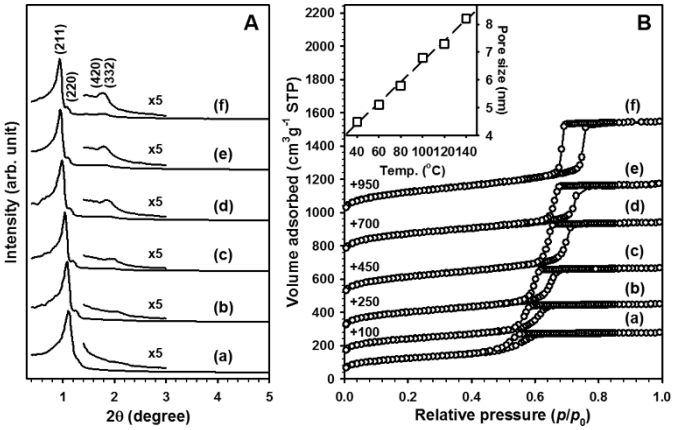

Fig. 1 Low and angle XRD patterns (A), and N_2 sorption isotherms (B) of the KIT-6-*t* silica templates where hydrothermal temperature *t* is equal to (a) 40 °C, (b) 60 °C, (c) 80 °C, (d) 100 °C, (e) 120 °C, and (f) 140 °C, respectively. Inset in (B) is the dependence of pore sizes of the KIT-6-*t* samples on the hydrothermal temperatures.

Table 1 Textural properties of the mesoporous silica KIT-6-*t*.

Material	S_{BET} [a] /m^2g^{-1}	V_{tot} [b] /cm^3g^{-1}	D_p [c] /nm	d_{211} [d] /nm	a_0 [e] /nm	T_w [f] /nm	$2T_w+D_p$ /nm
KIT-6-40	443.3	0.43	4.5	7.9	19.5	5.2	14.9
KIT-6-60	484.3	0.54	5.1	8.1	19.8	4.8	14.7
KIT-6-80	520.6	0.64	5.8	8.5	20.8	4.6	15.0
KIT-6-100	561.5	0.76	6.8	8.9	21.8	4.1	15.0
KIT-6-120	596.4	0.73	7.3	9.3	22.7	4.0	15.3
KIT-6-140	591.6	0.92	8.2	9.4	23.0	3.3	14.8

[a] Surface areas are calculated by using the BET method. [b] Total pore volumes of the materials were estimaed from the N_2 sorption isotherms at p/p_0 = 0.99. [c] Pore sizes were calculated from the adsorption branches of the N_2 sorption isothermss by using the BJH method. [d] d_{211}-spacing of the materials was obtained from the low angle XRD patterns using a Bragg's equation. [e] Unit cell parameters given by the $a_0 = d_{211}\sqrt{6}$. [f] The wall thickness was calculated by using the equation, $T_w = a_0/2 - D_p$.[50]

3.2 Effect of chemical composition

Highly ordered mesoporous CZS-100-*x* ternary compound semiconductors with well-developed crystalline frameworks were successfully synthesized *via* nano-replication method using 3-D bicontinuous cubic *Ia*3*d* mesostuructured KIT-6-100 as a hard template with cheap and easily available precursors. Simple impregnation with various molar compositions of the precursors within mesopores of the silica template, reduction at 500 °C under H_2 atmospheres and subsequent silica template etching process using NaOH aqueous solution resulted in the mesoporous $Cd_xZn_{1-x}Se$ materials.

Fig. 2 shows low and wide angle XRD patterns of the template-free ordered mesoporous CZS-100-*x* materials with various molar composition (x = 0 – 1). As shown in Fig. 2A, all of the materials exhibit same diffraction patterns with new peak at low angle region which corresponds to (110) plane. The presence of this new (110) diffraction peak means that mesostructure transformation of the CZS-100-*x* materials after the removal of KIT-6 silica template is occurred from cubic *Ia*3*d* to tetragonal $I4_1/a$ or lower symmetry.[23, 50-54] This mesostructure transformation upon the template removal is probably because CZS networks are only formed in one of the two chiral pore channels in the mesoporous silica template KIT-6 during the the high temperature reduction process of the precursors into the crystalline CZS. This mesostructure transformation was also investigated in the synthesis of mesoporous materials *via* nano-replication method such as carbons, metals, and metal oxides from the mesoporous silica MCM-48 which has cubic *Ia*3*d* meso-structures without interconnecting micropore channels and/or KIT-6 materials as hard-templates.[23, 50-54]

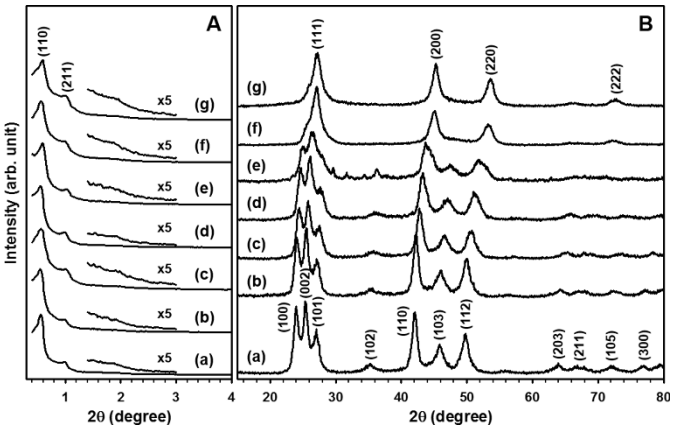

Fig. 2 Low (A) and wide (B) angle XRD patterns of the replicated ordered mesoporous CZS-100-*x* materials where *x* is equal to (a) 1.0 (CdSe), (b) 0.9, (c) 0.7, (d) 0.5, (e) 0.3, (f) 0.1, and (g) 0.0 (ZnSe), respectively.

The wide angle XRD patterns of the CZS-100-1.0 and CZS-100-0.0 have several peaks which correspond to wurtizte (hexagonal $P6_3mc$, PDF no. 08-0459) and zinc blende (cubic F-43m, PDF no. 05-0522) crystal structures (Fig. 2B). The calculated lattice parameters from the wide angle XRD patterns (a = 4.295 Å and c = 7.011 Å for CdSe in Fig. 2B (a); a = 5.667 Å for ZnSe in Fig. 2B (g)) are faithfully matched with the values given in JCPDS card (a = 4.299 Å and c = 7.010 Å for

CdSe in PDF no. 08-0459; a = 5.667 Å for ZnSe in PDF no. 05-0522). As shown in Fig. 2B, the ternary compound semiconductor materials, CZS-100-x, show periodical peak-shifting in their wide angle XRD patterns with the changes of the chemical composition x, due to difference in the atomic radius of cadmium and zinc. The crystal structures of the resulting CZS-100-x materials with relatively high cadmium composition (x = 0.3 – 0.9) exhibit similar XRD patterns to that of the wurtzite CdSe material. But, at much lower cadmium composition (x = 0.1), the crystal structure of the material is similar to that of the zinc blende ZnSe material. Also, the diffraction peaks of the CZS-100-x materials are gradually shifted to higher 2θ degrees at the cadmium composition x as goes to the lower values in the materials. These XRD peak-shifting represent that the crystal structures of the CZS-100-x materials are changed from wurtzite to zinc blende as the composition (x) in the CZS-100-x materials as goes from 1.0 to 0.0.

The highly ordered mesosturctures with uniform pore size and well-developed crystalline frameworks of the CZS-100-0.5 material were observed from TEM images (Fig. 3). The well-developed crystalline frameworks of the CZS-100-0.5 material was also observed in HR-TEM image (inset of Fig. 3c) and the d-spacing of 3.95 Å is correspond to (110) plane. Energy dispersed X-ray spectroscopy (EDS) mapping images (Fig. 3d, 3e and 3f) show that the cadmium, zinc and selenium elements in the resulting CZS-100-0.5 material are homogeneously dispersed over the whole particles. The elemental analysis also confirms that the atomic ratio between cadmium and zinc metals equal to 0.93 (21.7 at% of Cd and 23.7at% of Zn in CZS-100-0.5). As shown in Fig. S3 and Fig. S4 (see supplementary information), the CZS-100-x materials with different molar composition (x) also exhibit highly ordered mesostructures.

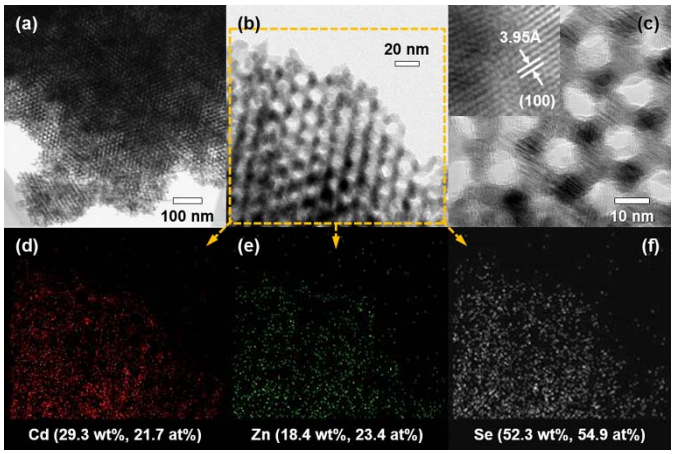

Fig. 3 TEM (a – c), HR-TEM (inset in c) and EDS mapping images (d – f) of the CZS-100-0.5 material for (d) Cd, (e) Zn and (f) Se, respectively.

The porosities of the mesoporous CZS-100-x materials were characterized by the N_2 adsorption-desorption measurement. All of the CZS-100-x materials showing typical type-IV with hysteresis loop in the range of p/p_0 = 0.8 – 1.0, which is the characteristic of the mesoporous material (Fig. 4A). The corresponding BJH pore size distributions of the CZS-100-x materials in Fig. 4B, which are obtained from the adsorption branches of the N_2-sorption isotherms, show the almost same mesopore size of 18 nm. The pore sizes of CZS-100-x materials are much larger than the silica framework thickness of the KIT-6-100 template (4.1 nm), regardless of chemical composition x changes in the material. These large mesopores of the CZS replicated materials also supports the phase-transformation from cubic $Ia3d$ to tetragonal $I4_1/a$ or lower symmetry of mesostructures which is expected from the low angle XRD patterns in Fig. 2A.

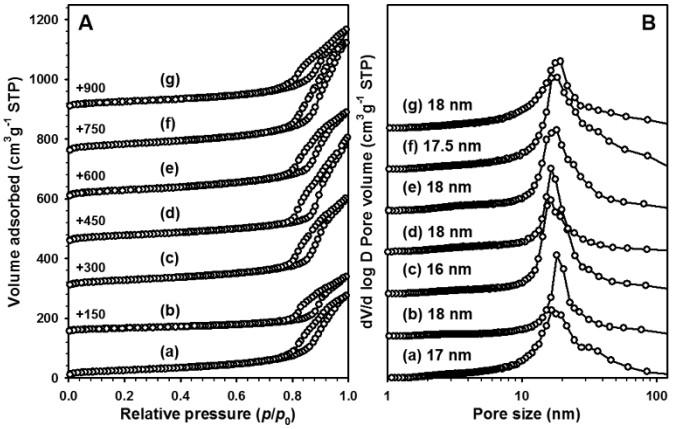

Fig. 4 N_2 sorption isotherms (A) and corresponding BJH pore size distributions of the replicated ordered mesoporous CZS-100-x materials where x is equal to (a) 1.0 (CdSe), (b) 0.9, (c) 0.7, (d) 0.5, (e) 0.3, (f) 0.1, and (g) 0.0 (ZnSe), respectively.

The unique optical properties of the CZS-100-x materials were characterized by the diffuse reflectance UV-visible spectroscopy and resulting spectra are shown in Fig. 5A. The absorption band of the CZS-100-x materials were periodically blue-shifted as impregnated cadmium precursor molar composition x as goes from 1.0 (CdSe) to 0.0 (ZnSe) because of their band gap energy changes. Fig. 5B represents Kubelka-Munk plots calculated by following equation from diffuse reflectance UV-visible spectra:

$$\mathrm{F}(R) = \frac{(1-R)^2}{2R}$$

where R is the reflectance.[55] The inset of Fig. 5B is the dependence of band gap energies of the CZS-100-x materials on composition. The band gap energies of mesoporous CdSe (CZS-100-1.0, 1.86 eV) and ZnSe (CZS-100-0.0, 2.44 eV) are larger than those of bulk CdSe (1.75 eV) and ZnSe (2.43 eV), respectively, due to the quantum confinement effect of nano-size frameworks. The band gap energies of ternary compound semiconductor materials (x = 0.1 to 0.9) which were obtained from the Kubelka-Munk plots are also slightly larger than those of calculated values given by Vegard's law:

$$E_g(A_xB_{1-x}C) = xE_g(AC) + (1-x)E_g(BC) - bx(1-x)$$

where *b* is the bowing parameter which also corresponds to nano-size effect, and almost lineally increased with composition *x* as goes from 0.0 to 1.0 as shown in inset of Fig. 5B and Table 2.[56-58] Because the Vegard's law is based on the bulk material, this band gap widening phenomenon also supports the CZS-100-*x* material has nano-domain size which could be confirmed from the XRD patterns and UV-visible spectra.

Interestingly, as shown in Fig. 5d, e and f, some of the CZS-100-*x* materials have shoulder peaks in diffuse reflectance UV-visible spectrums. The presence of these shoulder peak in the spectrum suggests that the compositional inhomogeneity is in existence at the ternary semiconductor frameworks of the replicated CZS-100-*x* material. Although all of elements homogeneously dispersed in whole particles in the TEM EDS mapping studies in Fig. 3d – 3f, compositional inhomogeneity of the frameworks exists in somewhere of bulk particles. The TEM studies is only limited to certain areas of the particles, UV-visible studies more reasonably adopted.

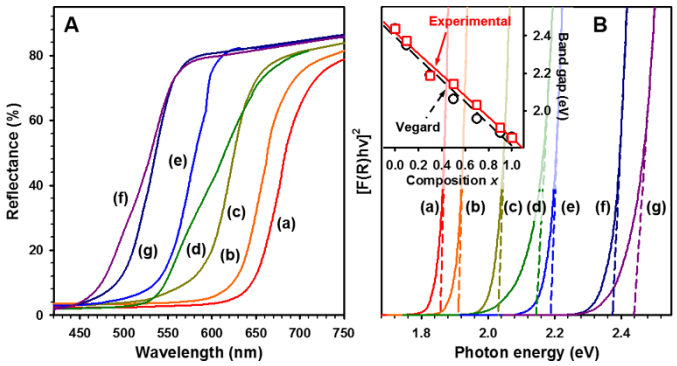

Fig. 5 UV-visible spectra (A) and corresponding Kubelka-Munk plots (B) of the mesoporous CZS-100-*x* materials where *x* is equal to (a) 1.0 (CdSe), (b) 0.9, (c) 0.7, (d) 0.5, (e) 0.3, (f) 0.1, and (g) 0.0 (ZnSe), respectively. Inset in (B) is the dependence of the band gap energy of CZS-100-*x* materials on composition estimated by the Vegard's law (○, black dotted line) and from the Kubelka-Munk plots (□, red solid line), respectively.

Table 2 Physical properties of the mesoporous CZS-100-*x* materials.

Material	S_{BET} /m^2g^{-1}	V_{tot} /cm^3g^{-1}	D_p /nm	a_0 [a] /nm	E_g [b] /eV
CZS-100-1.0	93.1	0.43	17	21.9	1.86
CZS-100-0.9	102.4	0.28	18	22.2	1.91
CZS-100-0.7	103.2	0.47	16	21.9	2.03
CZS-100-0.5	102.1	0.55	18	22.2	2.14
CZS-100-0.3	107.8	0.48	18	20.8	2.19
CZS-100-0.1	122.6	0.58	17.5	22.2	2.37
CZS-100-0.0	116.3	0.54	18	21.2	2.44

[a] Unit cell parameters given by the $a_0 = d_{110}\sqrt{2}$. [b] Band gap energies estimated from the Kubelka-Munk plots in Fig. 5B.

3.3 Effect of framework thickness

As discussed in above section, band gap engineering of the mesoporous CZS-100-*x* materials possible through the chemical composition control of the frameworks, and obtained mesoporous semiconductor materials exhibit larger band gap energies than bulk materials. We expect that this band gap widening phenomenon would be related to the quantum confinement effect, due to nano-sized frameworks. So, to study about relationship between the band gap energy and framework thickness, we design the framework size controlled mesoporous CZS-*t*-0.5 materials.

The CZS-*t*-0.5 materials, which were obtained from the KIT-6-*t* templates with different mesopore sizes, have ordered mesostructures and high crystallinities (Fig. 6). The (110) peak of the CZS-*t*-0.5 materials in Fig. 6A is gradually shifted to lower angles from (a) CZS-40-0.5 to (g) CZS-140-0.5. This peak shifting in low angle XRD patterns is related to the wall thickness changes of the CZS-*t*-0.5 material.[49] In spite of the pore size and/or wall thickness differences of the silica templates, all CZS-*t*-0.5 materials show same mesostructures, and the mesostructures of the CZS-*t*-0.5 materials more and more ordered when they were synthesized from the silica template KIT-6 with higher and higher hydrothermal temperatures (Fig. 6A).

The wide-angle XRD patterns in Fig. 6B show several diffraction peaks in the range of 22 – 30 °, indicating that all the CZS-*t*-0.5 materials exhibit almost same wurtzite-like crystal structure which is similar to that of wurtzite CdSe (JCPDS PDF no. 08-0459). The smaller mesopore size of the silica template KIT-6-*t* results thinner framework size of the replicated CZS-*t*-0.5 material, and gives broader peaks in wide XRD patterns. The estimated grain sizes by using Scherrer's equation from XRD peaks between 22 – 30 ° after decombolution processes gradually increased from 4.2 to 8.2 nm with the increases of the pore size of silica template from 4.5 to 8.2 nm (Table 3).

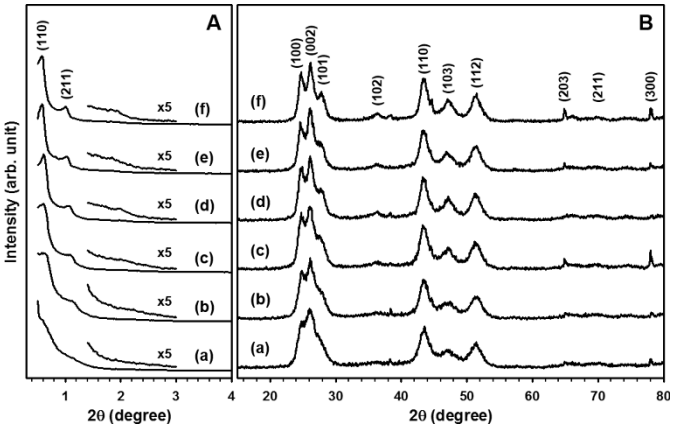

Fig. 6 Low (A) and wide (B) angle XRD patterns of the ordered mesoporous CZS-*t*-0.5 materials where *t* is equal to (a) 40, (b) 60, (c) 80, (d) 100, (e) 120, and (f) 140, respectively.

The N_2 adsorption-desorption isotherms and corresponding BJH pore size distributions of the mesoporous CZS-*t*-0.5 materials are shown in Fig. 7. All of the CZS-*t*-0.5 materials exhibit typical type-IV isotherms with hysteresis loop in the range of $p/p_0 = 0.8 – 1.0$. Interestingly, in spite of different pore size of silica template KIT-6, resulting CZS-*t*-0.5 materials have similar mesopore size in the range of 15 – 18 nm. Because the only one of the two chiral pore channels is filled by the precursor solution and resulting single gyroid structure of the CZS-*t*-0.5 material, the space occupied by two walls and one

mesopore of the KIT-6 are converted into the mesopores of the framework of the replica sample. The calculated spaces ($2T_w + D_p$) of the silica template KIT-6 are very similar to each other (Table 1), and this is why the resulting mesoporous CZS-*t*-0.5 materials exhibiting similar mesopore sizes. The mesopore sizes of resulting CZS-*t*-0.5 materials slightly larger than calculated spaces of the silica template (around 15 nm) because the frameworks of the CZS-*t*-0.5 were not faithfully filled in the mesopore of the silica template during the impregnation processes by using incipient wetness method due to the presence of solvent molecules, and crystalline wall volume of the materials shrunk during the crystallization process. Similar to CZS-100-*x* materials, the CZS-*t*-0.5 also exhibits high surface areas of about 100 m^2g^{-1}, and have no tendency of pore volume changes by pore size and/or volume changes of the silica templates.

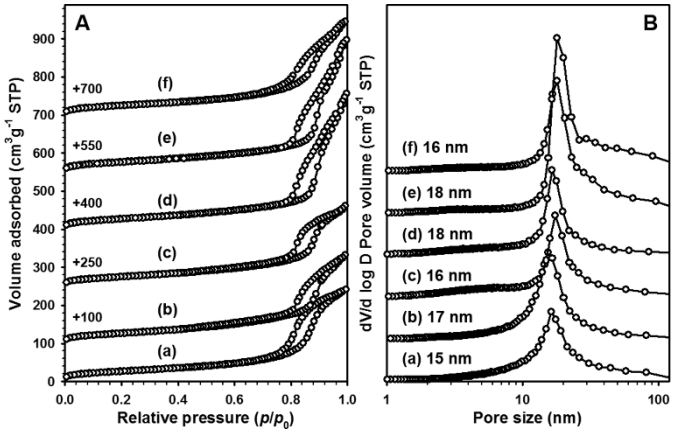

Fig. 7 N_2 sorption isotherms (A) and corresponding BJH pore size distributions (B) of the ordered mesoporous CZS-*t*-0.5 materials where *t* is equal to (a) 40, (b) 60, (c) 80, (d) 100, (e) 120, and (f) 140, respectively.

The wall thicknesses of the CZS-*t*-0.5 material measured from the HR-TEM images (insets in Fig. 8) were steadily increased from 5.5 to 6.8 nm with the increases of the mesopore sizes of the silica template KIT-6 as goes from 5.1 to 8.2 nm, except the CZS-40-0.5 material (measurement of the wall thickness of CZS-40-0.5 material is very hard from there HR-TEM image). The tendency of the increases of wall thickness (from HR-TEM images) and grain size (from the wide angle XRD patterns) supports the framework size of the resulting material can be easily controlled by using pore size controlled silica template, KIT-6-*t*. The mesopore sizes of the CZS-*t*-0.5 materials in TEM images are similar to each other regardless of hydrothermal temperature *t* which can be also confirmed from the BJH pore size distributions in Fig. 7B. The more ordered mesostructures of the CZS-*t*-0.5 materials at the higher hydrothermal temperature *t* also could be observed in the TEM images (Fig. 8) which is corresponds to the low angle XRD patterns in Fig. 6A.

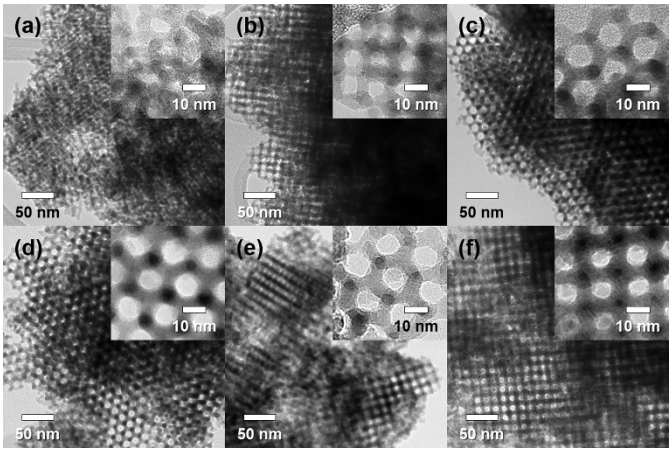

Fig. 8 TEM images of the ordered mesoporous CZS-*t*-0.5 materials where *t* is equal to (a) 40, (b) 60, (c) 80, (d) 100, (e) 120, and (f) 140, respectively. Inset is the HR-TEM image.

As depicted in diffuse reflectance UV-visible spectra (Fig. 9A), absorption bands of the CZS-*t*-0.5 materials slightly red-shifted from 550 to 600 nm as the framework thickness increases (i.e., hydrothermal temperature *t* of silica template KIT-6-*t* increases from 40 to 140 °C). Due to the framework sizes of the CZS-*t*-0.5 material were controlled in nano-meter scale, the energy spectrum turns to discrete, and as a result, the band gap energies become size dependent which called as nano-size effect. The nano-size effect results in band gap energy widening and blue-shift in optical illumination at the wall thickness decreases of the materials.

The Kubelka-Munk plots depicted in Fig. 9B supports the nano-size effect of CZS-*t*-0.5 material as discussed above. The calculated band gap energies decreased with the increases of wall thickness of the CZS-*t*-0.5. Because the both crystallite size and wall thickness of the CZS-*t*-0.5 material increase, the band gap energies estimated from the Kubelka-Munk plots gradually decrease from 2.17 to 2.04 eV.

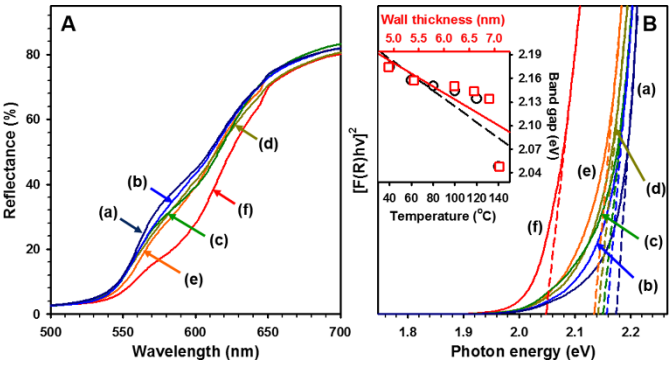

Fig. 9 UV-visible spectra (A) and corresponding Kubelka-Munk plots (B) of the mesoporous CZS-*t*-0.5 materials where *t* is equal to (a) 40, (b) 60, (c) 80, (d) 100, (e) 120, and (f) 140, respectively. Inset in B is the dependence of band gap energy of CZS-*t*-0.5 material on hydrothermal temperature of silica template KIT-6s (○, black dotted line) or wall thickness (□, red solid line) estimated from the Kubelka-Munk plots.

Table 3 Physical properties of the mesoporous CZS-*t*-0.5 materials.

Material	S_{BET} /m^2g^{-1}	V_{tot} /cm^3g^{-1}	D_p /nm	τ [a] /nm	T_w [b] /nm	E_g [c] /eV
CZS-40-0.5	98.3	0.37	15	4.2	-	2.17
CZS-60-0.5	100.2	0.36	17	5.2	5.5	2.16
CZS-80-0.5	95.5	0.34	16	5.8	5.8	2.14
CZS-100-0.5	102.1	0.55	18	6.0	6.0	2.12
CZS-120-0.5	100.9	0.53	18	6.5	6.5	2.10
CZS-140-0.5	104.8	0.38	16	6.8	6.8	2.04

[a] Crystallite sizes of the materials were calculate by Scherrer's equation. [b] Wall thickness of the materials estimated from the HR-Tem images in Fig. 8 inset. [c] Band gap energies estimated from the Kubelka-Munk plots in Fig. 9B.

4. Conclusion

We report on a facile synthesis route to highly ordered mesoporous $Cd_xZn_{1-x}Se$ ternary compound semiconductor materials with crystalline frameworks *via* nano-replication method using a bicontinuous 3-D cubic *Ia3d* mesoporous silica KIT-6 template with controlled pore sizes from 4.5 to 8.2 nm as hard-templates. The optical properties of the replicated template-free $Cd_xZn_{1-x}Se$ ternary semiconductor materials were chemically and physically controlled by control of the chemical composition of the precursors and by using a pore size controlled mesoporous silica KIT-6 as a hard-template. The present band-gap engineering, based on chemical and physical methods, enables a design of compound semiconductor materials with crystalline frameworks, ordered mesostructures and unique optical properties.

Acknowledgements

This work was supported by a grant of the Korean Health Technology R&D Project, Ministry of Health & Welfare, Republic of Korea (No. HN10C0005). J.M.K also thanks the Energy Efficiency & Resources Core Technology Program of the Korea Institute of Energy Technology Evaluation and Planning (KETEP) granted financial resource from the Ministry of Trade, Industry & Energy (No. 20132020000260) and the Basic Science Research Program through the National Research Foundation of Korea (NRF) funded by the Ministry of Education (2012R1A6A1040282).

Notes and references

[a] *SKKU Advanced Institute of Nanotechnology, Sungkyunkwan University, Suwon 440-746, Republic of Korea.*
[b] *Department of Chemistry, Sungkyunkwan University, Suwon 440-746, Republic of Korea. Fax: +82 31 299 4174; Tel: +82 31 290 5930; E-mail: jimankim@skku.edu*
[c] *Department of Energy Science, Sungkyunkwan University, Suwon 440-746, Republic of Korea.*
[d] *Amorepacific R&D Center, Yongin 446-729, Republic of Korea.*
[e] *Department of Semiconductor Systems Engineering, School of Information and Communication Engineering, Sungkyunkwan University, Suwon, 440-746, Republic of Korea.*
[‡] *Present address: Energy Lab., Samsung Advanced Institute of Technology (SAIT), Samsung Electronics Co., Ltd., P.O. Box 111, Suwon 440-600, Republic of Korea. Tel: +82 31 8061 1259; E-mail: jk78.shon@samsung.com*

† Electronic Supplementary Information (ESI) available: BJH pore size distribution curves, TEM and SEM images. See DOI: 10.1039/b000000x/

1 Y. Xia, P. Yang, Y. Sun, Y. Wu, B. Mayers, B. Gates, Y. Yin, F. Kim and H. Yan, *Adv. Mater.*, 2003, **15**, 353-389.
2. A. K. Geim and K. S. Novoselov, *Nature Materials*, 2007, **6**, 183-191.
3. A.-H. Lu, E. L. Salabas and F. Schüth, *Angew. Chem. Int. Ed.*, 2007, **46**, 1222-1244.
4. J. Park, J. Joo, S. G. Kwon, Y. Jang and T. Hyeon, *Angew. Chem. Int. Ed.*, 2007, **46**, 4630-4660.
5. A. Corma, *Chem. Rev.*, 1997, **97**, 2373-2420.
6. J. Y. Ying, C. P. Mehnert and M. S. Wong, *Angew. Chem. Int. Ed.*, 1999, **38**, 56-77.
7. A. Hagfeldt and M. Grätzel, *Acc. Chem. Res.*, 2000, **33**, 269-277.
8. M. E. Davis, *Nature*, 2002, **417**, 813-821.
9. Y. Zhao, L. Xu, L. Mai, C. Han, Q. An, X. Xu, X. Liu and Q. Zhang, *Pro. Natl. Acad. Sci.*, 2012, **109**, 19569-19574.
10. J. S. Beck, J. C. Vartuli, W. J. Roth, M. E. Leonowicz, C. T. Kresge, K. D. Schmitt, C. T. W. Chu, D. H. Olson and E. W. Sheppard, *J. Am. Chem. Soc.*, 1992, **114**, 10834-10843.
11. C. T. Kresge, M. E. Leonowicz, W. J. Roth, J. C. Vartuli and J. S. Beck, *Nature*, 1992, **359**, 710-712.
12. G. S. Attard, J. C. Glyde and C. G. Goltner, *Nature*, 1995, **378**, 366-368.
13. Q. Huo, D. I. Margolese and G. D. Stucky, *Chem. Mater.*, 1996, **8**, 1147-1160.
14. D. Zhao, J. Feng, Q. Huo, N. Melosh, G. H. Fredrickson, B. F. Chmelka and G. D. Stucky, *Science*, 1998, **279**, 548-552.
15. H. I. Lee, J. H. Kim, G. D. Stucky, Y. Shi, C. Pak and J. M. Kim, *J. Mater. Chem.*, 2010, **20**, 8483-8487.
16. J. Qi, H. Nan, D. Xu and Q. Cai, *Cryst. Growth Des.*, 2011, **11**, 910-915.
17. P. Yang, D. Zhao, D. I. Margolese, B. F. Chmelka and G. D. Stucky, *Nature*, 1998, **396**, 152-155.
18. R. Ryoo, S. H. Joo and S. Jun, *J. Phys. Chem. B*, 1999, **103**, 7743-7746.
19. S. H. Joo, S. J. Choi, I. Oh, J. Kwak, Z. Liu, O. Terasaki and R. Ryoo, *Nature*, 2001, **412**, 169-172.
20. R. Ryoo, S. H. Joo, M. Kruk and M. Jaroniec, *Adv. Mater.*, 2001, **13**, 677-681.
21. D. E. De Vos, M. Dams, B. F. Sels and P. A. Jacobs, *Chem. Rev.*, 2002, **102**, 3615-3640.
22. S. S. Kim, H. I. Lee, J. K. Shon, J. Y. Hur, M. S. Kang, S. S. Park, S. S. Kong, J. A. Yu, M. Seo, D. Li, S. S. Thakur and J. M. Kim, *Chem. Lett.*, 2008, **37**, 140-141.
23. J. K. Shon, S. S. Kong, J. M. Kim, C. H. Ko, M. Jin, Y. Y. Lee, S. H. Hwang, J. A. Yoon and J.-N. Kim, *Chem. Commun.*, 2009, 650-652.
24. J. K. Shon, S. S. Kong, Y. S. Kim, J.-H. Lee, W. K. Park, S. C. Park and J. M. Kim, *Micropor. Mesopor. Mater.*, 2009, **120**, 441-446.
25. H. Wang, H. Y. Jeong, M. Imura, L. Wang, L. Radhakrishnan, N. Fujita, T. Castle, O. Terasaki and Y. Yamauchi, *J. Am. Chem. Soc.*, 2011, **133**, 14526-14529.
26. H. Wang, Y. Teng, L. Radhakrishnan, Y. Nemoto, M. Imura, Y. Shimakawa and Y. Yamauchi, *J. Nanosci. Nanotechno.*, 2011, **11**, 3843-3850.
27. H. Wang, M. Imura, Y. Nemoto, S.-E. Park and Y. Yamauchi, *Chem. – Asian J.*, 2012, **7**, 802-808.

28. P. Karthika, H. Ataee-Esfahani, H. Wang, M. A. Francis, H. Abe, N. Rajalakshmi, K. S. Dhathathreyan, D. Arivuoli and Y. Yamauchi, *Chem. –Asian J.*, 2013, **8**, 902-907.
29. T. Trindade, P. O'Brien and N. L. Pickett, *Chemistry of Materials*, 2001, **13**, 3843-3858.
30. W. U. Huynh, X. Peng and A. P. Alivisatos, *Adv. Mater.*, 1999, **11**, 923-927.
31. L. Manna, E. C. Scher and A. P. Alivisatos, *J. Am. Chem. Soc.*, 2000, **122**, 12700-12706.
32. W. U. Huynh, J. J. Dittmer and A. P. Alivisatos, *Science*, 2002, **295**, 2425-2427.
33. L. Manna, D. J. Milliron, A. Meisel, E. C. Scher and A. P. Alivisatos, *Nat. Mater.*, 2003, **2**, 382-385.
34. B. Sun, E. Marx and N. C. Greenham, *Nano Lett.*, 2003, **3**, 961-963.
35. D. J. Milliron, S. M. Hughes, Y. Cui, L. Manna, J. Li, L.-W. Wang and A. Paul Alivisatos, *Nature*, 2004, **430**, 190-195.
36. I. Gur, N. A. Fromer, C.-P. Chen, A. G. Kanaras and A. P. Alivisatos, *Nano Lett.*, 2006, **7**, 409-414.
37. M. J. MacLachlan, N. Coombs and G. A. Ozin, *Nature*, 1999, **397**, 681-684.
38. F. Gao, Q. Lu and D. Zhao, *Adv. Mater.*, 2003, **15**, 739-742.
39. Y. Shi, Y. Wan and D. Zhao, *Chem. Soc. Rev.*, 2011, **40**, 3854-3878.
40. V. I. Klimov, A. A. Mikhailovsky, S. Xu, A. Malko, J. A. Hollingsworth, C. A. Leatherdale, H.-J. Eisler and M. G. Bawendi, *Science*, 2000, **290**, 314-317.
41. S. Coe, W.-K. Woo, M. Bawendi and V. Bulovic, *Nature*, 2002, **420**, 800-803.
42. Z. H. Ni, H. M. Fan, J. Kasim, Y. M. You, Y. P. Feng, M. Y. Han and Z. X. Shen, *J. Phys.: Condens. Matter*, 2008, **20**, 325214.
43. M. R. Kim, S.-Y. Park and D.-J. Jang, *Adv. Funct. Mater.*, 2009, **19**, 3910-3916.
44. N. C. Greenham, X. Peng and A. P. Alivisatos, *Synthetic Met.*, 1997, **84**, 545-546.
45. X. Wu, Y. Yu, Y. Liu, Y. Xu, C. Liu and B. Zhang, *Angew. Chem. Int. Ed.*, 2012, **51**, 3211-3215.
46. X. Zhong, Z. Zhang, S. Liu, M. Han and W. Knoll, *J. Phys. Chem. B*, 2004, **108**, 15552-15559.
47. R. Zhang and P. Yang, *Journal of Physics and Chemistry of Solids*, 2013, **74**, 759-764.
48. F. Kleitz, S. Hei Choi and R. Ryoo, *Chem. Commun.*, 2003, 2136-2137.
49. T.-W. Kim, F. Kleitz, B. Paul and R. Ryoo, *J. Am. Chem. Soc.*, 2005, **127**, 7601-7610.
50. L. A. Solovyov, V. I. Zaikovskii, A. N. Shmakov, O. V. Belousov and R. Ryoo, *J. Phys. Chem. B*, 2002, **106**, 12198-12202.
51. M. Kaneda, T. Tsubakiyama, A. Carlsson, Y. Sakamoto, T. Ohsuna, O. Terasaki, S. H. Joo and R. Ryoo, *J. Phys. Chem. B*, 2002, **106**, 1256-1266.
52. Z. Li, G. D. Del Cul, W. Yan, C. Liang and S. Dai, *J. Am. Chem. Soc.*, 2004, **126**, 12782-12783.
53. G. S. Armatas, A. P. Katsoulidis, D. E. Petrakis, P. J. Pomonis and M. G. Kanatzidis, *Chem. Mater.*, 2010, **22**, 5739-5746.
54. E. Kang, S. An, S. Yoon, J. K. Kim and J. Lee, *J. Mater. Chem.*, 2010, **20**, 7416-7421.
55. P. Kubelka and F. Munk, *Z. Tech. Phys.*, 1931, **12**, 593-610.
56. A. R. Denton and N. W. Ashcroft, *Phys. Rev. A*, 1991, **43**, 3161-3164.
57. H. C. Poon, Z. C. Feng, Y. P. Feng and M. F. Li, *J. Phys.: Condens. Matter*, 1995, **7**, 2783.
58. D. S. Sutrave, G. S. Shahane, V. B. Patil and L. P. Deshmukh, *Mater. Chem. Phys.*, 2000, **65**, 298-305.